An experimental Investigation into the surface and hydrodynamic characteristics of marine coatings with mimicked hull roughness ranges

Taylor & Francis
Taylor & Francis Group

Biofouling
The Journal of Bioadhesion and Biofilm Research

ISSN: 0892-7014 (Print) 1029-2454 (Online) Journal homepage: https://www.tandfonline.com/loi/gbif20

An experimental investigation into the surface and hydrodynamic characteristics of marine coatings with mimicked hull roughness ranges

I. A. Yeginbayeva & M. Atlar

To cite this article: I. A. Yeginbayeva & M. Atlar (2018) An experimental investigation into the surface and hydrodynamic characteristics of marine coatings with mimicked hull roughness ranges, Biofouling, 34:9, 1001-1019, DOI: 10.1080/08927014.2018.1529760

To link to this article: https://doi.org/10.1080/08927014.2018.1529760

Published online: 11 Dec 2018.

BIOFOULING
2018, VOL. 34, NO. 9, 1001–1019
https://doi.org/10.1080/08927014.2018.1529760

Taylor & Francis
Taylor & Francis Group

An experimental investigation into the surface and hydrodynamic characteristics of marine coatings with mimicked hull roughness ranges

I. A. Yeginbayeva[a] and M. Atlar[b]

[a]Department of Mechanics and Maritime Sciences (M2), Chalmers University of Technology, Gothenburg, Sweden; [b]Department of Naval Architecture, Ocean and Marine Engineering, University of Strathclyde, Glasgow, UK

ABSTRACT

There are limited scientific data on contributors to the added drag of in-service ships, represented by modern-day coating roughness and biofouling, either separately or combined. This study aimed to gain an insight into roughness and hydrodynamic performance of typical coatings under in-service conditions of roughened ships' hull surfaces. Comprehensive and systematic experimental data on the boundary layer and drag characteristics of antifouling coating systems with different finishes are presented. The coating types investigated were linear-polishing polymers, foul-release and controlled-depletion polymers. The data were collected through state-of-the-art equipment, including a 2-D laser Doppler velocimetry (LDV) system for hydrodynamic data in a large circulating water tunnel. Three coating systems were first applied on flat test panels with 'normal' finishes in the first test campaign to represent coating applications under idealised laboratory conditions. In order to address more realistic roughness conditions, as typically observed on ships' hulls, 'low' and 'high' roughness densities were introduced into the same types of coating, in the second test campaign. The data collected from the first test campaign served as the baseline to demonstrate the effect on the surface roughness and hydrodynamic drag characteristics of these coating types as a result of 'in-service' or 'severely flawed' coating application scenarios. Data collected on coatings with a range of in-service surface conditions provided a basis to establish correlation between the surface roughness characteristics and hydrodynamic performance (roughness function). The findings of the study indicate that the estimations of drag penalties based on well-applied, relatively smooth coating conditions underestimate the importance of hull roughness, which although undesirable, is commonplace in the world's commercial fleet.

ARTICLE HISTORY
Received 23 November 2017
Accepted 21 September 2018

KEYWORDS
Zero-pressure turbulent boundary layers; marine coatings; hull roughness; mimicked hull roughness; coatings; 'in-service' condition; skin friction drag

Introduction

Importance of hull roughness

In the natural environment and in engineering applications, turbulent boundary layer flows develop under the influence of surface characteristics. An important engineering application is the flow over ships' hulls, where the hull roughness or, in most cases, the coating condition becomes critically important. Especially for new-built ships, assumptions regarding hull roughness significantly influence the power required to drive the ship and thus its fuel consumption, as well as the initial and operational costs of the ship. Since the coating roughness changes continuously during the service life of a ship, it continues to receive attention both in experimental and theoretical studies. Although a great deal of data exist for roughness and hydrodynamic performance of newly applied coatings, data on coating performance under in-service conditions are scarce, especially for modern-day commercial coatings. Extensive research remains to be carried out to understand the hydrodynamic performance of coatings under in-service conditions, in order to improve estimates of associated ship power increases. This is also of utmost importance because of increasing environmental concerns associated with greenhouse gas (GHG) emissions due to maritime transport and the important role of marine coatings over the lifetime of ships (IMO 2009).

Currently, hull roughness is measured during in-docking and out-docking of vessels and is a major factor in forecasting ship efficiency. In the marine industry, R_t50 (the maximum peak-to-trough height taken over 50 mm sample length) has been adopted as a measure of hull roughness. This measure, in μm, is

CONTACT I. A. Yeginbayeva irmay@chalmers.se

obtained using the British Maritime Technology (BMT) hull roughness analyser (HRA) or Thermimport Quality Control (TQC) hull roughness gauge. Typically, several R_t50 values are taken at particular locations on the hull and combined to give a mean hull roughness (MHR) for that location. By combining MHR values from other hull locations into a single parameter or average hull roughness (AHR), the hull condition for a vessel at a particular time is quantified. When shipbuilders claim low fuel consumption, they assume and attempt to achieve lower AHR values. In essence, hull roughness of a ship in-service can be viewed as either physical roughness, such as substratum waviness, damage, corrosion and coating characteristics, or as biological roughness, which is caused by the attachment of marine organisms when exposed to water. According to O'Leary and Anderson (2003), each roughness has its own associated micro- and macro-scale characteristics. Without considering biological roughness, physical roughness itself is still not well understood. Macro-physical roughness usually accounts for the longer wavelength roughness features of the hull ($L_c \geq 50$ mm) associated with plate waviness, plate laps, seams and butts, welds and weld quality, mechanical damage and the underlying substratum profile. On the other hand, the micro-physical roughness accounts for the shorter wavelength roughness features ($L_c \leq 10$ mm) and is typically attributable to minor corrosion, and coating characteristics, type and condition (Stenson et al. 2013).

For hydrodynamically smooth hull surfaces, roughness elements are normally smaller than the thickness of the viscous sublayer within the turbulent boundary layer. However, when the roughness element is bigger than the viscous sublayer, the layer is unable to mask the peaks comprising roughness element, thus resulting in increased friction. Taking into account the fact that the viscous sublayer gets thinner with increasing vessel speed, Nakao (1988) suggested that the desirable hull roughness is ~10–30 μm in order to ensure that roughness elements are not protruding above the viscous sublayer. Ideally, hull roughness is preferred to be lower than the desirable hull roughness value. With currently existing materials and application procedures, the AHR for new ships can be <125 μm with higher and lower limits of 100 μm and 75 μm respectively (Berendsen 2013). Obviously, the AHR values for in-service ships are even higher than 125 μm. If shot-blasted and primed new steel hulls usually have mean roughness values in the range of 40–50 μm, this means that another ≈80 μm of excess roughness is added for the new ship by the subsequent paint layers. However, by following some quality control measures and improved personnel skills, AHR values of <75 μm can be achieved in practice. Still, this value is higher than the desirable roughness. In the context of the impact of current coating systems on the AHR, a study by Stenson et al. (2014) presents the analysis of a new dataset of roughness surveys carried out between 2003 and 2014 on 283 ships in dry-dock. This dataset shows that an AHR of >200 μm, although undesirable, is relatively commonplace in the world's commercial shipping fleet. The higher frequency in AHR readings is encountered for the typical coatings of the controlled-depletion polymer (CDP) type than for coatings of the self-polishing copolymer (SPC) and foul-release (FR) types.

Identification of causes of hull roughness

There are many processes that, taken singly or in combination, create hull roughness. These may be conveniently divided into two phases: (1) occurring at the pre-delivery stage and (2) occurring on ships in service, including routine dry-docking. The initial extra roughness identified by AHR measurements is influenced by the condition of the hull prior to coating application. This condition can be affected by poor fabrication works and any subsequent events associated with inadequacy in field application of coatings such as berthing and poor application standards. As a result, newly applied coating finishes may be rougher than the ideal, because of poor coating application procedures such as curtaining, sagging, overspray and the inclusion of dust and grit (B.S.R.A. 1980). In addition, during in-service operation of the vessels, multiple factors such as coating technology, vessel type and trading route are likely to be highly correlated to each other and further drive the initial ship hull roughness. Firstly, the roughness of the coatings may subsequently increase due to coating wear, contact damage and premature failures, which are associated with hull service conditions. Secondly, antifouling provision may gradually become inadequate, which results in development of microfouling (eg light biofilm (slime)) and progressive hard fouling (eg weed, barnacles), forming a complex and diverse community (Dürr & Thomason 2010). It is not possible to identify the single parameter responsible for the increase in AHR values and predict the ship performance based on simple, linear models. Therefore, practical approaches need to be developed to successfully mimic the conditions experienced by hull coatings in real or in-service conditions. It is also important to point out that ships with a higher initial

roughness roughen at a higher rate than ships with a lower initial roughness (Berendsen 2013). Therefore, careful attention should be given specifically to hull surface preparation and coating application. The lower initial AHR can be achieved by quality control of coating operations, improved training of application personnel, provision of adequate access to the hull and protection from the weather during coating application.

Effect of hull roughness on ship resistance

Detrimental effects, which occur during the life-cycle of the coatings, influence the roughness, integrity and effectiveness of the coatings. These effects lead to powering penalties for the shipping industry: speed loss while maintaining a constant ship power and vice versa (Haslbeck & Bohlander 1992; Townsin 2003; Schultz 2007); increased fuel consumption and hence GHG emission (IMO 2009); poor manoeuvrability performance; increased dry-docking time; and associated manpower and cost. Hull roughness measured during the 1980s on ships of various ages indicated that a rate of 25 μm year^{-1} in AHR increase was typical. Using this hull roughness deterioration rate, AHR values for three, six and nine-year-old ships with an assumption of initial hull roughness values of new ships will be 200, 275, 350 μm, respectively. However, AHR observed during the 2003–2014 surveys by International Paint Ltd (Gateshead, Tyne and Wear, United Kingdom) revealed only a modest impact of vessel age on AHR. As an example, a mean AHR increase with time since dry-dock of 0.84 μm month^{-1} (≈10 μm year^{-1}) was observed across the unfiltered raw data (Stenson et al. 2014). This decrease in the rate of AHR increase over the intervening decades may be explained by the combination of improvements made in ship manufacturing process, coating application process as well as in maintenance procedures in the shipping industry.

A considerable amount of work has been performed in the field of coating hydrodynamic performance, mainly for newly applied coatings. For test surface preparation, coatings are usually applied to a well-established substratum by well-maintained equipment under controlled conditions which are free from operational and atmospheric influences. Thus, laboratory coating application represents an idealised scenario. In reality, progressively greater roughness is observed for coating applied under field conditions. One of the pioneering works, which provided a systematic set of data on drag, boundary layer and roughness of modern-day marine antifouling (AF) surfaces was carried out by Candries (2001). Another study, which contributed to further understanding of state-of-the-art rough-wall turbulent boundary layer flows over marine AF coatings, can be found in Unal B (2012). Schultz and Flack (2003) investigated the effect of roughness ranges on flat-plate turbulent boundary layers. In their experimental work, acrylic plates were painted with several coats of marine polyamide epoxy paints and tested in terms of roughness and drag characteristics under the following three conditions: unsanded, wet sanded with 60-grit and with 120-grit sandpaper. As a result of comparisons of turbulent boundary layers developing over painted surfaces smoothed by sanding with smooth reference, Schultz and Flack (2003) observed increases in boundary layer parameters together with a downward shift in velocity profiles for the unsanded, painted surface compared with smooth wall data. This study also gave an insight into the detrimental effect of sandgrain roughness on the surface roughness and the skin friction coefficients. Recent towing tank experiments carried out by Savio et al. (2015) looked at the effects of different quality of paint application on the roughness and frictional drag characteristics. The authors defined the term 'paint' as the epoxy primer coat used for the final coat; however, this does not represent a typical underwater coating system, which has multiple layers of anticorrosive and AF coats. Although this kind of surface has been studied many times, to the present authors' best knowledge, no marine paints with AF binding agents have been tested to investigate the effect of different roughness or the quality of paint application.

As noted previously, there is a lack of investigations of surface roughness and frictional resistance performance of commercial hull coatings in-service conditions. 'In-service' hull conditions are assumed here to be partly represented by increased hull roughness and partly by biofouling (mainly biofilm) effects. This paper presents details and results of hull roughness effects in the absence of biofilms as one of the major contributors to the in-service condition. For this purpose, hull roughness that can be observed on ship hulls at micro- and macro- levels were mimicked in combination with three types of commercial antifouling coatings. This should enable estimation of the hull frictional resistance and projected power requirements based on a more realistic dataset. This is noteworthy since current values of in-service roughness and associated power requirements needed to overcome resistance are often estimated and are

approximate due to a lack of scientific data, as presented in this paper. The results of this study can also be used as an input to Computational Fluid Dynamics (CFD) studies to enhance the development of numerical approaches to the problem.

Materials and methods

Test facility and experimental set-up

Boundary layer experiments with flat acrylic test panels in uncoated and coated conditions were conducted in the Emerson cavitation tunnel (ECT) of Newcastle University (UNEW), UK. The ECT is a closed-circuit depressurised tunnel with a measuring section of 3.10 m × 1.22 m × 0.81 m and a contraction ratio of 4.27:1. More detailed information on the specification of the ECT and recent modernisations can be found in Atlar and Seo (2011).

The 'high-speed insert' installed in the measuring section of the tunnel was used as a test bed for boundary layer measurements over flat test panels. As shown in Figure 1a, whilst the insert accelerated the flow in the measuring section due to reduced cross-section, it also allowed a testing panel, which is called the UNEW standard test panel, to be fitted onto a slot to facilitate the boundary layer experiments. The velocity in the tunnel test bed was in the practical range of 0–6.0 m s^{-1}, whilst the turbulence intensity levels for the streamwise (U) and wall-normal (V) velocities were 2.75% and 3.75%, respectively (Korkut 1999). The side walls and floor of the tunnel's measuring section provided optical access.

In all laboratory-based experimental tests, it is important to ensure that the flow over the test panel is fully turbulent since the flow around the hull is turbulent. For this reason, a 400-mm wide strip with sand roughness CAMI grit 36 was located at a distance of 58 mm from the leading edge of the insert to trip the flow, as shown in Figure 1.

The test panels were designed to be flush with the surface of the insert to ensure a zero streamwise pressure gradient (ZPG). Figure 1b shows the process mounting for the coated panel onto the test bed using six wing-nuts. Shims were used, when needed, to align the test panels flush with the insert. Figure 1b shows the top view of the tunnel's measuring section; the coated panel is on the right side of the tunnel's main axis so that laser Doppler velocimetry (LDV) beams can access the tunnel's measuring section through the bottom optical window. Velocity-time data for test surfaces were collected using a two-dimensional DANTEC's FiberFlow LDV system with a Fiber PDA 58N70 detector unit (DANTEC 2007). Velocity profiles in the streamwise (U) and wall-normal directions (V) were measured using green ($\lambda = 514.5$ nm) and blue ($\lambda = 488$ nm) beams respectively at three freestream velocities (nominally 2, 4 and 6 m s^{-1}) and at position 1 only (POS1), which corresponds to 2.7 m (or $\approx 61\delta$) from the leading edge of the tunnel insert. Selection of these three velocities, within the capability of the ECT, was based on following: the highest freestream velocity (6 m s^{-1}) was preferred for more realistic Reynolds number representation. Operation of the ECT at this top speed is not always practical due to vibrations, heat, high energy and cost. Therefore, a moderate freestream velocity (4 m s^{-1}) was also included as a compromise, which still offers a good indication of the Reynolds number effect.

In the present study, the test bed was found to produce ZPG boundary layers by observing the acceleration parameter (K) which was calculated using the equation given in Volino et al. (2007). For all test cases K was less than 1.85×10^{-8}. Patel (1965) observed that substantial deviation from the logarithmic law of the wall occurred for values of $K > 1.6 \times 10^{-6}$.

Test surfaces

Coatings were applied to flat test panels to measure their boundary layer characteristics in the ECT. The standard test panel had a length (L) of 0.6 m and a width (W) of 0.22 m. The base for all panels was manufactured from Perspex acrylic.

Three class of coating products, *viz.* Intersleek® 1100SR, Intercept® 8000 LPP and Interspeed® 6400, which represent respectively typical examples of foul-release (FR), linear-polishing polymer (LPP) and controlled-depletion polymer (CDP) systems, were studied systematically in terms of their surface roughness and hydrodynamic drag characteristics during two experimental campaigns. Although the Intercept® 8000 LPP brand is no longer commercially available, the concept continues to be promoted for Intercept® 8500 LPP and its fouling control principle is similar to that of typical self-polishing copolymers (SPC). All coatings from both campaigns consisted of a full coating scheme which included the application of an anti-corrosive primer coat, tie coat and finish coat. The application of coatings on standard panels was accomplished in the laboratories of International Paint Ltd. Variations in humidity and temperature were eliminated by applying candidate coatings

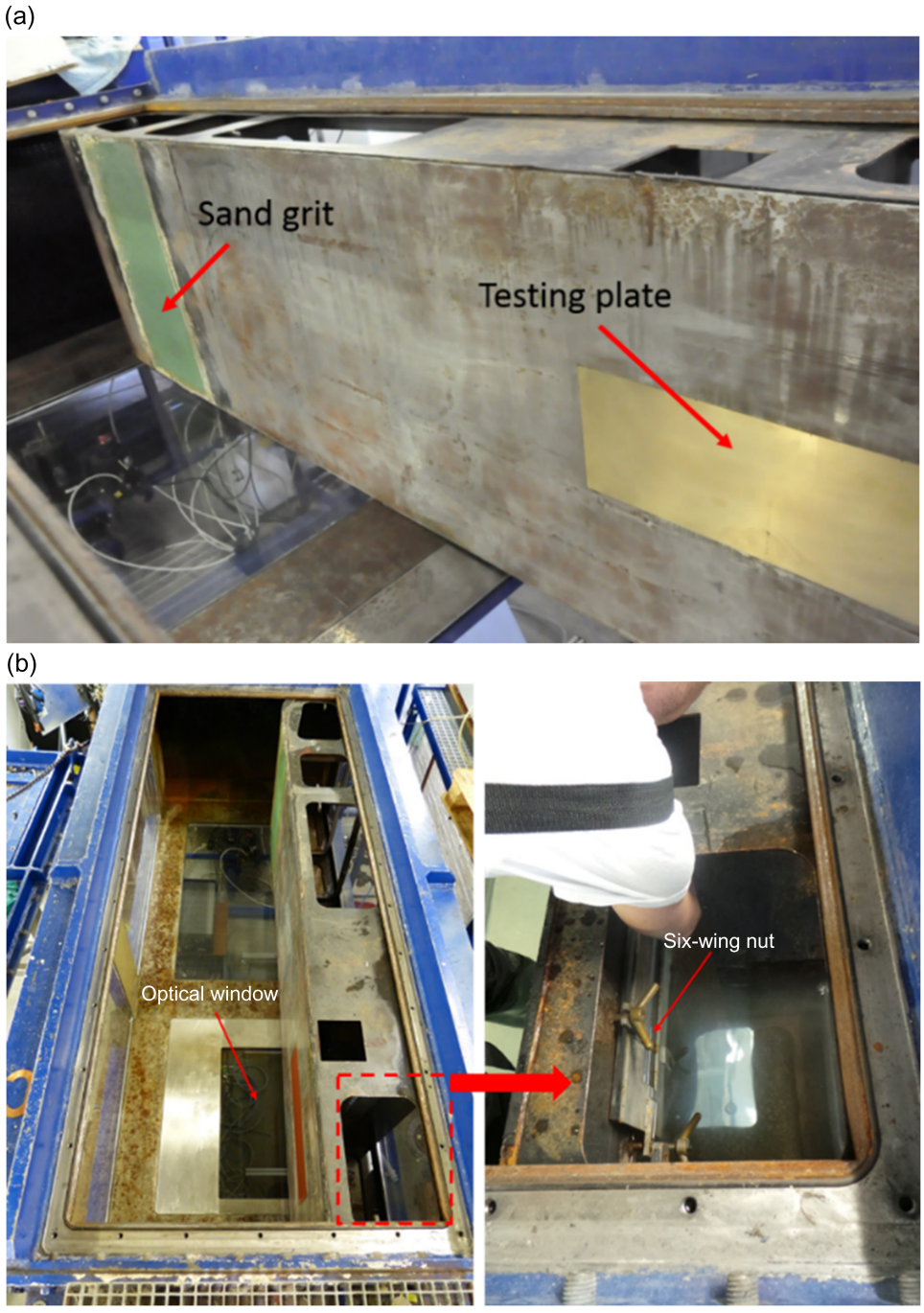

Figure 1. Photograph of a 'high-speed insert' (test bed) with flush mounted test panel installed in the Emerson cavitation tunnel's testing section (a); top view of a test bed and test panel mounting (b).

indoors in a temperature-controlled paint spray booth. Variations in the application were minimised by using the same 'hopper' gun, which is usually used to apply deck coatings on vessels.

Coatings in the first test campaign included FR, LPP and CDP types applied onto UNEW test panels with a clean acrylic base using standard application procedures by spraying. These are specified as 'normal' finish (or application) coatings representing clean coatings at best or in their idealised laboratory-applied conditions. Each coating application was made in triplicate, which resulted in nine panels being used as the first test campaign test surfaces.

To investigate the performance of coatings under in-service conditions, an approach been successfully developed to mimic the levels of physical roughness experienced on real ships' hulls in service; this was based on the experience of International Paint Ltd and their analysis of a dataset of 845 individual hull roughness surveys carried out between 2003 and 2014

by Stenson et al. (2014). To begin the application process to mimic hull roughness ranges of ships, artificial roughness in the form of sand grit of 25 and 50% by weight was introduced into the anticorrosive coats of the FR, LPP and CDP systems respectively. These two different sand grit levels were assumed to represent 'low' and 'high' densities of hull roughness scenarios. Before the coating application, acrylic base panels were abraded with sandpaper to roughen the surface and allow the anticorrosive coat to better adhere. After leaving the anti-corrosive to cure for a day, the panels were overcoated with tie-coats and finish coats. FR, LPP and CDP with two percentage of grit weight were produced, yielding a total of six low and six high densities of hull roughness representatives to be tested as part of a second campaign designated 'second test campaign'. These coated panels, which mimic in-service hull roughness were referred to as mimicked hull finishes.

The first campaign of experiments with the normal finish served as the baseline studies, whilst the second campaign of experiments demonstrated the effect of in-service or real-life coating conditions on the surface roughness and hydrodynamic characteristics of three types of coatings.

The surface roughness characteristics for the first and second test campaign panels were measured using a highly accurate, non-contact optical profile meter (UNISCAN OSP100A Laser Profilometer, Uniscan Instruments Ltd, a Bio-Logic SAS company, Seyssinet-Pariset 38170 FRANCE). Roughness data was taken over an area of $60 \times 90\,\text{mm}^2$. A total of 120 profiles with a 90 mm sampling length and a 25 µm sampling interval were obtained on each coated panel. The gathered roughness data were saved in 'txt' format and analysis of roughness profiles were carried out by using in-house analysis software. Surface waviness was removed using 5 mm long wavelength filtering. The amplitude and hybrid roughness parameters were calculated according to the definitions given by Dey (1989).

In addition to the above non-contact measurements, only the surface of mimicked hull roughness coated panels from the second test campaign was measured by using a contact stylus type hull roughness gauge (TQC). This was done to be able to relate to industry standard AHR or R_t50, against which a ship's performance is usually correlated. Ten repeat measurements were collected for each panel in the direction of the panel's length. The measurement of roughness toward the centres of the panels was intentionally avoided in order to minimise the possible effect on hydrodynamic drag.

Throughout this paper, the first, second and third replicate of typical FR, LPP and CDP coating types with the normal finish (the first test campaign) are specified as FR-rep1, FR-rep2, FR-rep3, LPP-rep1, LPP-rep2, LPP-rep3 and CDP-rep1, CDP-rep2, CDP-rep3 respectively.

The first replicate of typical FR, LPP and CDP coating types with low and high roughness densities (the second test campaign) are denoted as FR-low1, LPP-low1, CDP-low1 and FR-high1, LPP-high1 and CDP-high1, respectively. The names for the second replicate of the same coating types for the second test campaign follow the same as previous coating identifiers: FR-low2, LPP-low2, CDP-low2 and FR-high2, LPP-high2, CDP-high2.

Additional surface data with an area of $25 \times 25\,\text{mm}^2$ were also gathered using the Optical Surface Profilometer (OSP) for the coatings from both campaigns in order to generate 3-D topographical views as presented in Figure 2. Close inspection of these topographies showed that the FR type coatings vary greatly from other coated surfaces. The FR coated panels, both in normal and mimicked hull finish application scenarios (Figure 2 from left to right), demonstrate small-scale peaks and valleys compared to LPP and CDP types.

Determination of the friction velocity

The Krogstad's method was used to estimate the friction velocities and to produce non-dimensional velocity profile plots for the tested surfaces. This method assumes the existence of log-law and the wake region of the velocity profile and it is fundamentally based on the iterative least-squares optimisation procedure for the three unknowns such as the friction velocity (u_τ), the wake parameter (Π) and the error in origin (ε). It involves examination of the velocity profile plotted in the velocity defect region at a range $0.1 < y/\delta < 1$ (Krogstad et al. 1992). In this method, the wake parameter is not a fixed value as in other profile matching methods such as Hama's velocity defect law (Hama 1954).

Uncertainty estimates

An uncertainty assessment study was conducted based on the Coleman and Steele (1999) methodology. Precision based uncertainty estimates for the velocity measurements were achieved through repeated tests. Six replicate LDV measurements were carried out for the hydrodynamically smooth acrylic panel and

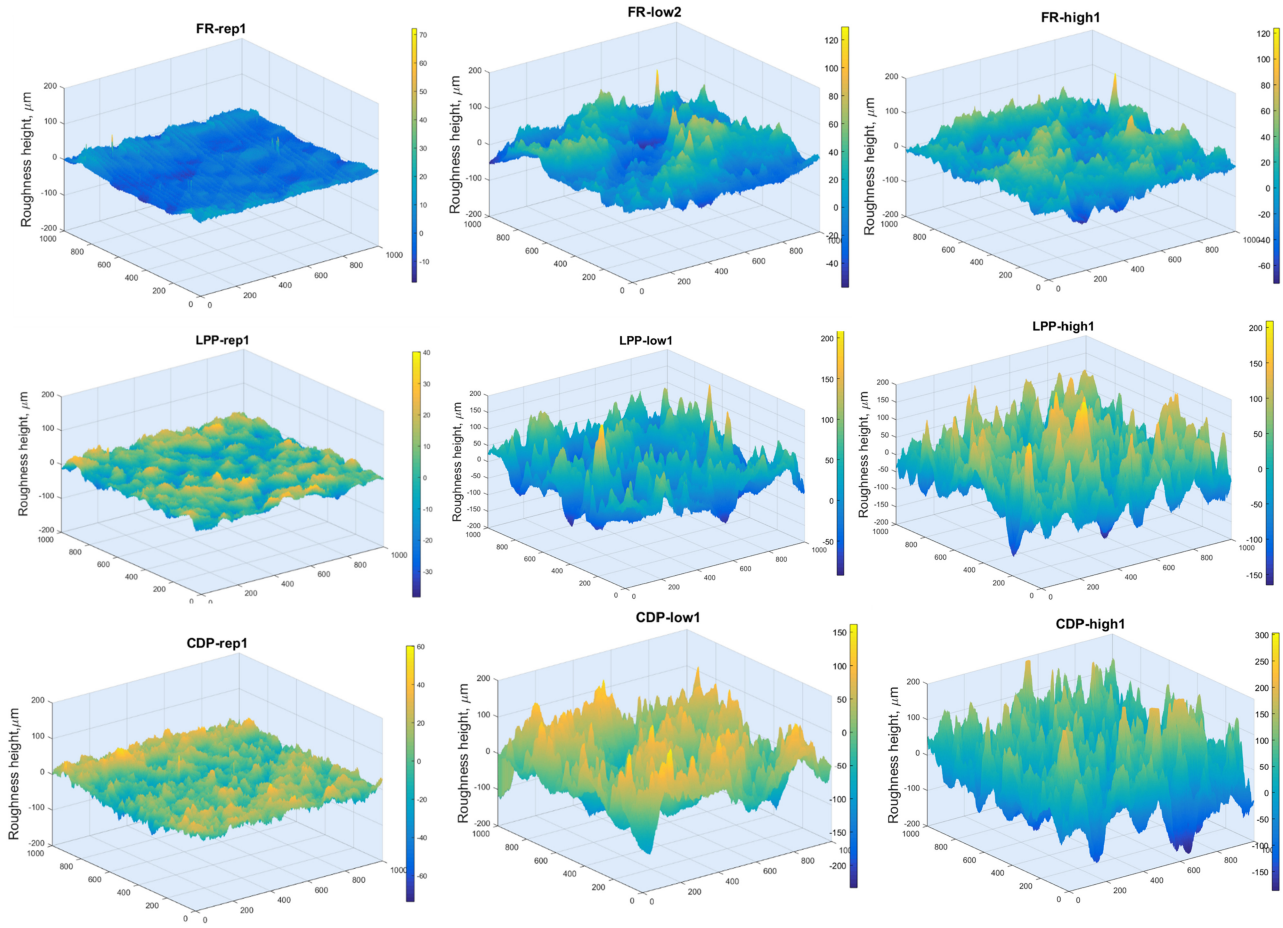

Figure 2. Topographical views of one replicate of each FR, LPP and CDP types with normal *vs* mimicked hull finishes. Plots from left to right represent the roughness densities. The surface texture measurement was taken at a $25 \times 25\,mm^2$ area with a sampling interval of 25 μm using an optical surface profilometer.

FR-rep1 at POS1. Measurement point numbers were kept the same as for the routine experimental set-up, namely, 57 points over the turbulent boundary layer. This number of points was found to be sufficient to achieve the constant freestream velocity in the ECT. The *t*-value for 95% confidence level and six repeated measurements were taken to be equal to 2.571 according to the statistical table for a two-tailed *t*-distribution (Swinscow & Campbell 2002). The maximum uncertainty level in the streamwise (U) velocity component for $\frac{y}{\delta} < 0.05$ was about 9%. This slightly high value can be due to the reflection of beams off the test panels. The uncertainty value reduced as the freestream velocity was approached. For most of the boundary layer, $\frac{y}{\delta} > 0.1$, the uncertainty in the streamwise velocity, U, accounted for 1%. The uncertainty levels for the friction velocity (u_τ) and local skin friction coefficients (C_f) using the Krogstad's method for the acrylic reference panel were calculated to be 1.08% and 2.15%, whereas for the FR panel these values were 1.33% and 2.66%, respectively.

Results and discussion

Coatings roughness analysis

The roughness data of the coated panels used in the first and second test campaigns and measured by the OSP and TQC hull roughness gauges are presented in detail in Yeginbayeva (2017). The amplitude (R_a (μm) – mean/average roughness; R_q (μm) – root mean square roughness; R_t (μm) – maximum peak-to-trough height; S_k – skewness; Ku – kurtosis), the spacing (S_m – mean spacing), and the hybrid parameters (S_a (°) – mean absolute slope angle; λ_a (mm) – average wavelength of a profile) were calculated for each test panel to characterise surface topography.

Amongst the first campaign of tested surfaces, replicates of the FR type systems (FR-rep1, FR-rep2, FR-rep3) were found to be the smoothest (ie $R_a \approx 2.0\,\mu m$), while CDP coating replicates (CDP-rep1, CDP-rep2, CDP-rep3) were the roughest (ie $R_a \approx 8.0\,\mu m$). The roughness of LPP-rep1, LPP-rep2, LPP-rep3 was ranked in between the smoothest and roughest coatings (ie $R_a \approx 4.5\,\mu m$).

Average roughness values (R_a) for the second test campaign coatings ranged from 6.30 µm to 28.83 µm. It has been noticed that depending on low and high density of physical roughness in the coating scheme, the values of amplitude parameters were low and high, respectively. However, FR type coatings with the low and high densities of roughness seem to have less pronounced effects compared to LPP and CDP types. Grouping of surfaces prepared for the second test campaign showed significant differences within the replicates of FR, LPP and CDP types with mimicked low roughness densities. However, good repeatability in R_a and R_q parameters was achieved for FR, LPP types with mimicked high roughness densities. Therefore, given the variability in substratum roughness, most of the coated panels should be considered as unique.

According to measurement results obtained from the TQC hull roughness gauge (2018), maximum peak-to-trough height measured over a 50 mm sample length or R_t 50 of coatings with mimicked hull roughness varied from 197 µm to 333 µm. This range covers the global AHR dataset for 'seriously flawed' coating application collected during 2003–2014 by International Paint Ltd (Stenson et al. 2014). In contrast, the R_t 50 values of all the normal finish panels prepared in this study ranged from 40 µm to 50 µm which, in the authors' experience, is typical for laboratory-applied panels without artificially enhanced roughness.

Mean velocity profiles

Using the LDV, boundary layer measurements were taken over nine and 12 coated panels prepared with the normal and mimicked hull roughness finishes, respectively. The Reynolds number based on the momentum thickness for the reference smooth test panel varied from $Re_\theta = 7{,}500$ to $Re_\theta = 22{,}000$.

The basic boundary layer parameters (such as boundary layer thickness, δ; displacement thickness, δ^*; momentum thickness, θ; inflow velocity, U_e; Reynolds number based on the boundary layer momentum thickness, Re_θ; friction velocity, u_τ; subsequent skin friction coefficient, C_f; and roughness functions, ΔU^+) for 21 coated panels of the first and second test campaigns were calculated and presented in Yeginbayeva (2017). The boundary layer data for FR coating with a low density of sand grit (FR-low1) were lost during the test campaign and therefore the data are missing for FR-low1 in subsequent plots.

For the sake of brevity and clarity, Figure 3 presents only the mean velocity profiles of the tested coatings with mimicked hull roughness using inner scaling (normalised by u_τ and ν/u_τ) for three incoming flow speeds (nominally 2, 4 and 6 m s^{-1}). Also shown for comparison are the results of the smooth acrylic reference surface.

In Figure 3a and b, the mean streamwise velocity profiles for the first and second replicates of coatings containing low and high densities of mimicked hull roughness are compared with profiles for the acrylic reference data. From Figure 3a it can be observed that the mean velocity profiles for the first replicate of each LPP and CDP coatings with low level of hull roughness clearly show a smaller downward shift, hence they have the less drag as opposed to the second replicates of the same coating types with the same roughness presented in Figure 3b. The second replicates of LPP and CDP types with both low and high level of mimicked roughness exhibit similar downward shift in velocity profiles. Therefore, similar drag is plausible for the second replicates of low and high densities of mimicked roughness in the FR, LPP and CDP coatings, which are discussed in a following section on roughness functions.

Skin friction data

Figure 4 shows the variation of skin friction coefficient, C_f, with Reynolds number based on momentum thickness, Re_θ. The skin friction coefficient of the smooth acrylic reference is compared to the experimental data of DeGraaff (1999), who presented a comprehensive study on flat-plate boundary layers over a wide range of Reynolds numbers ($1{,}500 < Re_\theta < 31{,}000$). The graph shows that the reference acrylic data very closely follow the data of DeGraaff for Reynolds numbers in the range of $7{,}400 < Re_\theta < 22{,}000$. Figure 4 also shows the variation of C_f for all the coatings with normal finish and low and high density of mimicked hull roughness ranges.

Figure 4 shows that increases in C_f due to different conditions were dependent on the coating type and roughness of the test surfaces. For example, the highest increase in C_f for FR, LPP and CDP type coatings applied by using normal finish were 4%, 11% and 13%, respectively. Further increases in C_f were observed for coated panels with the mimicked low and high hull roughness ranges typically observed on ship hulls. The roughness and drag measurements of the FR coated panels revealed that low and high mimicked roughness effects are less pronounced on these coating types. According to roughness analysis, roughness

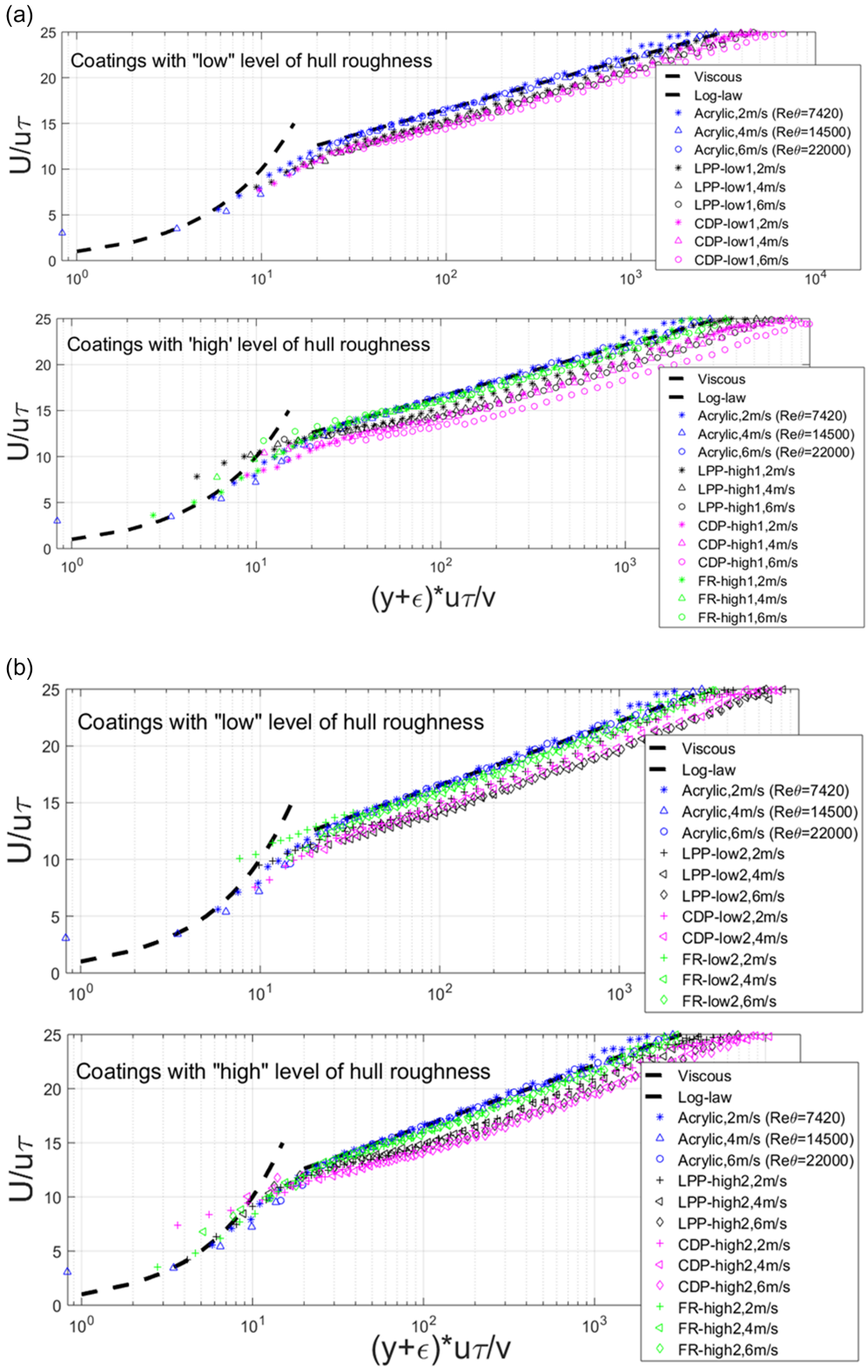

Figure 3. Mean streamwise velocity profiles of coated surfaces with different hull roughness densities. The first replicate of each FR, LPP and CDP coated surfaces with low and high hull roughness (a); the second replicate of each FR, LPP and CDP coated surfaces with low and high hull roughness (b).

parameters for FR replicates with high hull were not significantly different than FR with low roughness. Similarly, increases in C_f at the highest *Re* for 'FR-low2' and 'FR-high1', 'FR-high2' were very close, 8% and 9% respectively, when compared to the smooth wall data.

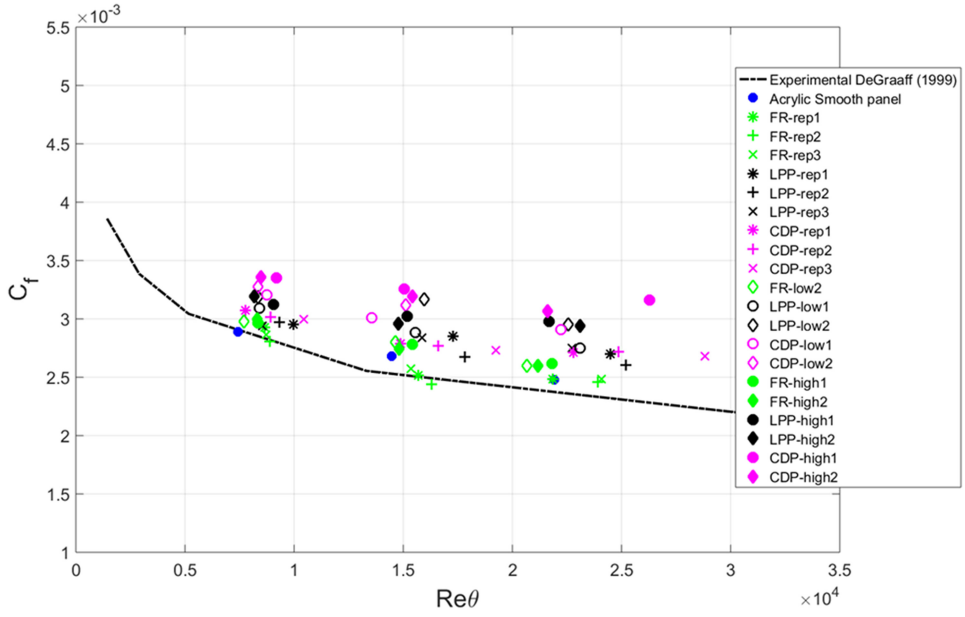

Figure 4. Variation in the skin friction coefficient (C_f) with Reynolds number (Re_θ) for the smooth reference, coatings with normal and mimicked hull finishes.

Amongst all the LPP and CDP coated surfaces with the 'low' density of roughness application, the maximum increase in C_f at moderate Reynolds number was found to be around 16% higher for LPP-low2 and CDP-low1 than the smooth reference. LPP-low2 at lower Reynolds number performs better compared to the other two high Reynolds numbers, displaying only 12% increase in the values of skin friction. However, with increasing Reynolds number, LPP-low2 showed rapidly increased drag. LPP-low1 seems to perform better than all of the other biocidal coatings and their replicates containing mimicked hull roughness ranges. This can be explained by the lower roughness characteristics. On average, an increase of just over 10% in skin friction was observed for LPP-low1 when compared to the smooth reference surface.

The highest increases in C_f were found for CDP and LPP coatings with the high level of introduced roughness. The maximum increases in C_f for CDP-high1 and CDP-high2 at the highest Reynolds number were found to be 25% and 22% respectively when compared to the reference surface. Replicates LPP-high1 and LPP-high2 displayed an increase of 19% compared to the smooth reference at the highest Reynolds number.

Roughness functions

Skin friction, which manifests itself through wall shear stress, provides useful information about the degree of interaction between the solid surface and viscous fluid. The surface roughness plays a key role in determining the character of the surface and how this interaction happens. In general, the effect of a rough wall on the turbulent boundary layer is manifested through increased wall shear stress and the shift in mean velocity profile. This effect is usually described in terms of the roughness function (ΔU^+), which represents the roughness-caused shift (note this shift is usually downward; however, some surfaces, eg riblets, exhibit a positive shift) and relies on the concept of similarity between a smooth and a rough wall. The roughness function is also critical in relating the laboratory collected drag data to the full-scale ship performance.

A preferred way of presenting the roughness function of a given surface is to plot this function against a roughness-based Reynolds number, $k^+ = \frac{kU_\tau}{\nu}$. Here k is the roughness length scale which can be a single parameter or a combination of parameters representing the roughness characteristics of the surface. The plot enables the investigator to look for a correlation between the surface and hydrodynamic characteristics. As far as roughness function correlation curves are concerned, the Colebrook line has been broadly accepted to describe the behaviour of naturally occurring engineering surfaces from smooth to fully rough regimes (Colebrook 1939). For engineering surfaces with irregular roughness structures, like ship hull surfaces, Grigson (1992) suggested a slightly modified version of the Colebrook formula. These roughness functions were widely used in the turbulent boundary layer studies including studies of marine coatings (eg Candries 2001; Schultz & Flack 2003; Schultz 2004;

Candries & Atlar 2005; Demirel et al. 2014; Unal 2015).

Medhurst (1989, 1990) stated that four general characteristics of roughness are likely to affect the roughness function: (1) a measure of the roughness scale, eg amplitude parameters; (2) a measure of a slope or sharpness of individual roughness elements; (3) a range of frequencies composing the roughness profile; and (4) long cut-off wavelength applied to a particular surface.

Musker (1977) found a good correlation for his pipe experiments by combining multiple surface characteristics such as root mean square roughness (R_q), mean slope angle (S_a), skewness or symmetry (S_k) and kurtosis or sharpness of the roughness elements (Ku) as the measure of the roughness length scale, k. Since the work of Musker (1977), it has been understood generally that two statistical parameters such as height and texture are needed to characterise the surface in order to correlate with the drag produced by the given surface. Generally, height, slope and curvature parameters are known to comprise the texture of the surfaces (Dey 1989).

As presented in the following section, roughness functions calculated for a normal finish and for mimicked hull conditions displayed a monotonic behaviour when plotted against the roughness Reynolds number, rather than the inflectional Nikuradse-type roughness function (Nikuradse 1933). Therefore, the monotonic curves of Colebrook (1939), and its modified form Grigson (1992), were selected for transitionally rough flow regimes. Firstly, the Musker's formula was used in this study for correlation of surface and drag characteristics of the presently tested surfaces since it satisfies the above statement made by Medhurst. The roughness length scale formula, ie $k = R_q(1 + 0.5S_a\ )(1 + 0.2S_k\ Ku)$, given by Musker was chosen in an attempt to collapse roughness functions onto a Colebrook-type Grigson line. However, the correlation was found unsatisfactory due to the fact that the roughness functions for coated surfaces were shifted upwards without collapsing onto a single line. This was believed to be due to the poor correlation between S_k and Ku. Flack and Schultz (2010) also found that the Musker's formula gave no significant improvements in correlating the roughness data with the frictional drag of three-dimensional, irregular surfaces.

In this study, roughness parameters such as R_a, R_q, R_t, S_a, λ_a were found to be correlated to each other with a coefficient of determination equal to R^2=0.99. Such good correlation between several roughness parameters indicates that these interrelated parameters can be used interchangeably. Hence these roughness parameters were employed, independently and in combination, to collapse the data for all the coating types tested, including their replicates, to the Grigson line as presented in Figures 5 and 6.

The first (a) and second plot (b) in Figure 5 show that the roughness correlations including the arithmetic mean, $0.6R_a$, and peak-to-trough height, $0.14R_t$, are reasonably good in collapsing the roughness function results of all tested coated panels onto a Grigson line in the transitional flow regime. The replicates of the FR-high1 and FR-high2 have similar roughness function shapes and almost collapse onto each other. This is expected, since the roughness parameter for these replicates were not significantly different. The change in $\Delta U^+$for FR-low2 is similar to that of the FR replicates with high roughness. In Figure 5 it is noticeable that LPP-low2, LPP-high1 and LPP-high2 have nearly the same ΔU^+values. Again, this can be explained by the similar roughness values observed for these coatings. This also means that roughness variability can be observed between LPP-low1 and LPP-low2, which explains the differences in their roughness functions. Regression analysis show that the coefficients of determination (R^2) for roughness correlations using $0.6R_a$ and $0.14R_t$ are 0.87 and 0.89 respectively. This implies that 87% and 89% of the total variation in ΔU^+in Figure 5a and b can be explained by the Grigson line. Similarly, Schultz (2004) found a satisfactory collapse onto the Grigson roughness function when $0.17R_a$ was used as a roughness scale for PDMS silicone, ablative copper, SPC copper and SPC TBT AF coatings in as-applied painted conditions. The discrepancy between the presently used roughness length scale, $0.6R_a$, and that used by Schultz (2004), $0.17R_a$, is believed to be due to the roughness filtering applied in this study.

Figure 6a shows the attempted correlation when different roughness length scales, namely the combination of root mean square roughness, R_q, and skewness parameter, S_k. The correlation equation, $k = AR_q\ (1 + S_k)^B$ was originally developed by Flack and Schultz (2010) to determine the equivalent sand roughness values for the fully rough regime. Figure 6a shows that further improved correlation can obtained using the above-mentioned roughness length scale for surfaces with mimicked hull roughness ranges only. This is expected, since these coatings with mimicked hull roughness ranges, which were generated by the introduction of sand grit elements, are very similar to the three-dimensional roughness tested by Flack and

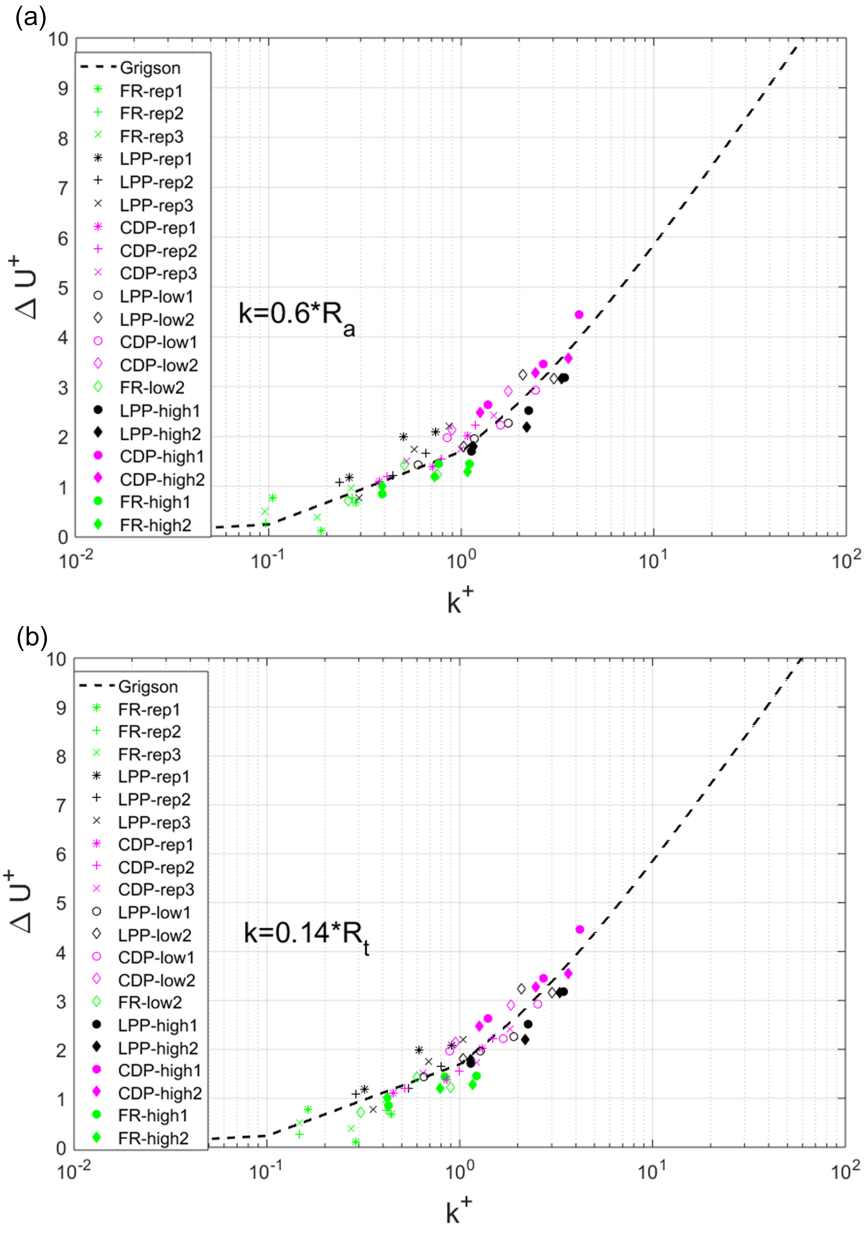

Figure 5. Roughness function results for FR, LPP and CDP types with normal and mimicked hull finishes: by using R_a (a) and R_t (b) calculated using a 5 mm cut-off length.

Schultz (2010), based on sandgrain, packed spheres and gravel covered with grit, etc. However, using the same roughness length scale was not adequate in obtaining a satisfactory collapse of the results for replicates of LPP and CDP types with normal applications. Agreement with the Grigson line was poor for these coatings, compared to previous correlations using single parameters like R_a and R_t. This is believed to be due to negative values of S_k only for replicates of LPP and CDP coatings with normal finish, thus implying that these surfaces exhibited more valleys than peaks. This study demonstrates that the as-applied antifouling coatings with a mild negative and even low skewness ($-0.14<S_k<0.01$) can reduce the goodness of fit. The coefficient of determination for Figure 6a was calculated as $R^2=0.62$. Flack and Schultz (2010) pointed out that more studies were needed, especially for surfaces with negative skewness, to validate and refine their correlation.

Figure 6b shows a further correlation study which was used with a combination based on interrelated parameters such as R_q and λ_a. The root mean square roughness parameter, R_q, was chosen from all of the amplitude parameters, as it is statistically significant according to Thomas (1999). Meanwhile, the average wavelength of a profile (λ_a) is analogous to the

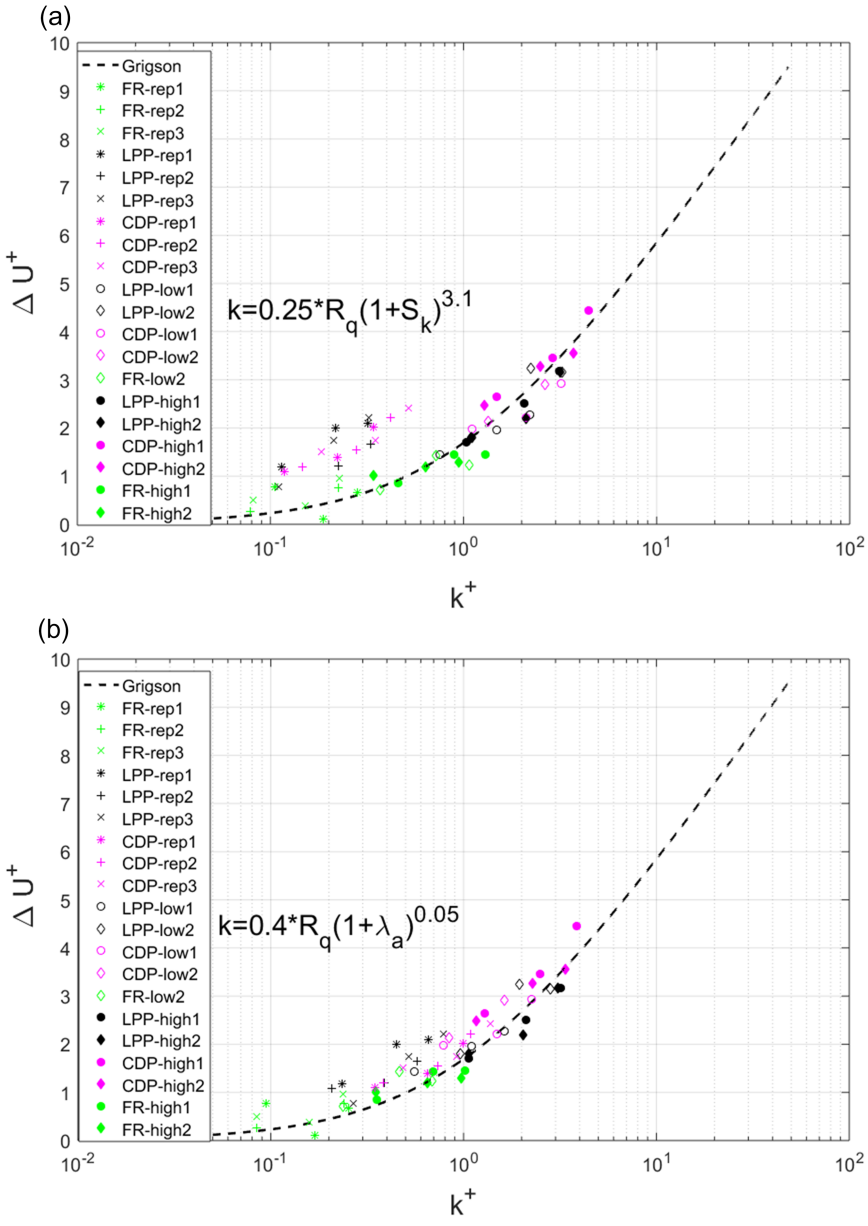

Figure 6. Roughness function results for FR, LPP and CDP types with normal and mimicked hull finishes: by using the Flack and Schultz (2010) equation (a), and by using a new correlation based on R_q and λ_a calculated using a 5 mm cut-off length (b).

average measure of a spatially predominant roughness wavelength. The average wavelength is also a reciprocal of the power spectral density (PSD), which in turn expresses the frequency content of the roughness profile obtained by a Fourier transform of the autocorrelation function (Bayer 1979). Normally, a higher magnitude in PSD indicates that a surface has a more 'open' texture. The average wavelengths (λ_a) for all test surfaces were calculated using Equation 1:

$$\lambda_a = \frac{2\pi\ R_a}{S_a} \tag{1}$$

where S_a is a mean absolute slope angle.

Figure 6b thus shows that the new correlation using R_q and λ_a parameters presented a much-improved correlation (R^2=0.75) compared to the equation proposed by Flack and Schultz (2010) for all FR, LPP and CDP type coatings with both normal and mimicked hull roughness ranges. Since the λ_a characterises the spatial distribution of the profile heights, it therefore provides a more representative description of the topography. The roughness function correlation in Figure 6b highlights the effectiveness of including the spatial distribution of roughness, and as such appears to be a key parameter in defining the flow character.

Table 1. Increase in frictional resistance, $\%\Delta C_F$, ΔC_F and effective power, $\%\Delta P_E$ for the KRISO container ship (KCS).

Ship type		KCS (L = 232.5m)					
Ship speed		(19 knots, Re = 1.73×10^9)			(24 knots, Re = 2.19×10^9)		
Description of condition		$\%\Delta C_F$	ΔC_F	$\%\Delta P_E$	$\%\Delta C_F$	ΔC_F	$\%\Delta P_E$
AF coatings with normal application	FR-rep1	1.74	0.000026	1.37	2.83	0.000040	1.94
	FR-rep2	1.53	0.000022	1.21	2.40	0.000034	1.65
	FR-rep3	1.50	0.000022	1.18	2.56	0.000036	1.76
	LPP-rep1	4.62	0.000068	3.65	5.75	0.000082	3.96
	LPP-rep2	3.89	0.000057	3.07	5.02	0.000072	3.45
	LPP-rep3	4.94	0.000073	3.90	6.30	0.000090	4.33
	CDP-rep1	6.10	0.000090	4.82	7.48	0.000107	5.14
	CDP-rep2	6.73	0.000099	5.32	8.53	0.000122	5.86
	CDP-rep3	8.06	0.000118	6.37	10.48	0.000150	7.21
AF coatings with mimicked low and high hull roughness densities	FR-low2	5.95	0.000087	4.70	6.80	0.000097	4.68
	FR-high1	8.56	0.000126	6.76	9.39	0.000134	6.46
	FR-high2	6.74	0.000099	5.33	8.94	0.000128	6.15
	LPP-low1	12.74	0.000187	10.07	12.80	0.000183	8.80
	LPP-low2	16.12	0.000237	12.74	16.96	0.000242	11.66
	LPP-high1	15.63	0.000229	12.35	15.90	0.000227	10.93
	LPP-high2	16.09	0.000236	12.72	16.33	0.000233	11.23
	CDP-low1	16.16	0.000237	12.77	16.33	0.000233	11.23
	CDP-low2	18.15	0.000266	14.34	18.66	0.000266	12.83
	CDP-high1	19.47	0.000286	15.39	19.58	0.000279	13.46
	CDP-high2	18.02	0.000265	14.24	18.01	0.000257	12.38

Effects of coating roughness on ship hull frictional resistance

In order to demonstrate the practical importance of the data presented in this paper, the laboratory analysis results obtained for three AF coatings were further used to predict the effect of normal and mimicked hull roughness densities on the frictional resistance and effective power of a representative ship in full-scale. The extrapolation from model scale to the full-scale ship is based on the flat-plate assumption and by using Granville's similarity law scaling procedure (Granville 1958), Granville 1987). A plot of C_F against Re for different ship lengths was obtained by following the algorithm given in Schultz (2007) for this scaling procedure. The procedure allows for the estimation of the effects of a particular surface roughness of flat plates on the frictional resistance of flat plates of ship length with the same roughness pattern.

For this extrapolation study, the benchmark KRISO Container Ship (KCS) (of the Korea Research Institute for Ships and Ocean Engineering) with a length of 232.5 m was used (Kim et al. 2001). There are several reasons behind the selection of this vessel. Firstly, KCS represents the modern hull of a container ship having a bulbous bow and stern and it has been widely used to derive experimental data such as resistance, mean flow, free surface waves and self-propulsion data (Hino 2005; Tezdogan et al. 2015) for CFD validation for this type of hull form (Larsson et al. 2014). Secondly, Demirel et al. (2017) predicted the effect of marine coatings and biofouling on the frictional resistance of this particular ship using a CFD based model and also presented the comparison of their enhanced results with the classical Granville-based predictions. Therefore, there is a good foundation for creating a database of KCS hull frictional resistance data for modern-day antifouling coatings with different surface roughness conditions as presented in this paper, so that results can be compared across independent studies.

Table 1 demonstrates the results of the extrapolation study and hence the practical implications for coatings of the FR, LPP and CDP types with normal and mimicked hull finishes for the resistance of this ship. The results are presented in terms of added frictional resistance (ΔC_F), subsequent percentage of this drag increase ($\%\ \Delta C_F$) and effective power increase ($\%\Delta P_E$). The full-scale predictions for the KCS hull were estimated for a waterline (WL) length of 232.5 m and wetted surface area of 9498 m^2 at two different service speeds, namely, its original design speed of 24 knots and an assumed slow-steaming speed of 19 knots. These speeds were also selected by Demirel et al. (2017) to investigate the effect of coatings and different range of biofouling on ship resistance using the roughness function values of Schultz and Flack (2007).

Depending on the coating type (ie FR, LPP or CDP), Table 1 shows that increases in the effective power for the KCS hull due to a normal finish application varied between 1.18% and 6.37% for 19 knots and between 1.65% and 7.21% for 24 knots. The hierarchy of the power increase related to the coating types was as follows: the minimum values were obtained for the

Table 2. Comparison of ΔC_F values calculated using the Bowden–Davison and Townsin formulae with the results of the current study.

Description of coating conditions	Bowden-Davison's equation A ΔC_F-1974	Townsin's equation B ΔC_F-1985-1 (19 knots)	Townsin's equation C ΔC_F-1985-2 (24 knots)	Current study results D ΔC_F (19 knots)	Current study results E ΔC_F (24 knots)	Percentage differences $\frac{\lvert A-D\rvert}{\frac{A+D}{2}}\times100$	Percentage differences $\frac{\lvert A-E\rvert}{\frac{A+E}{2}}\times100$	Percentage differences $\frac{\lvert B-D\rvert}{\frac{B+D}{2}}\times100$	Percentage differences $\frac{\lvert C-E\rvert}{\frac{C+E}{2}}\times100$
FR-low2	0.000354	0.000175	0.000202	0.000087	0.000097	121%	114%	67%	70%
FR-high1	0.000426	0.000205	0.000232	0.000126	0.000134	109%	104%	48%	54%
FR-high2	0.000412	0.000199	0.000227	0.000099	0.000128	123%	105%	67%	56%
LPP-low1	0.000370	0.000182	0.000209	0.000187	0.000183	66%	68%	3%	13%
LPP-low2	0.000484	0.000229	0.000257	0.000237	0.000242	68%	67%	3%	6%
LPP-high1	0.000497	0.000235	0.000262	0.000229	0.000227	74%	75%	2%	14%
LPP-high2	0.000519	0.000244	0.000272	0.000236	0.000233	75%	76%	3%	15%
CDP-low1	0.000457	0.000218	0.000246	0.000237	0.000233	63%	65%	8%	5%
CDP-low2	0.000457	0.000218	0.000246	0.000266	0.000266	53%	53%	20%	8%
CDP-high1	0.000535	0.000251	0.000278	0.000286	0.000279	61%	63%	13%	0%
CDP-high2	0.000544	0.000254	0.000282	0.000265	0.000257	69%	72%	4%	9%

FR type while the maximum values were for the CDP type. The values of the effective power increase with the mimicked hull roughness scenarios ranged from 4.7% to 15.39% for 19 knots and from 4.68% to 13.46% for 24 knots. The coating types showed the same trend as observed with the normal finish.

The results for the coatings with a normal finish agree well with previous studies for newly applied coating finishes. Predicted changes in the frictional resistance ($\%\Delta C_F$) for a container ship at 19 knots and 24 knots indicate that only a small increase (1.7% and 2.8% respectively) is expected from FR type coating with normal or relatively smooth conditions as compared to the hydraulically smooth hull. This compares well with widely used estimate given in Schultz (2007), who also observed only a small resistance penalty (≈2%) for typical, as-applied AF coatings with an equivalent sand grain roughness height of 30 µm. Whereas with mimicked hull roughness ranges, the same FR type coating showed quite a significant drag penalty (≈6.8% to 9.4% increases in ΔC_F). The $\%\Delta C_F$ values for LPP coatings with a normal finish at 19 knots and 24 knots are 4.9% and 6.3% respectively, whereas for CDP types with a normal finish $\%\Delta C_F$ values are 8.06% and 10.48% at the corresponding speeds. Predicted added drag values ($\%\Delta C_F$) of typical LPP and CDP type coatings with normal finish (including their replicates) were close to the results which Demirel et al. (2017) predicted for the same hull with typical AF coatings with 'as newly applied' conditions. Their predictions reported a 6.3% and 9% added drag ($\%\Delta C_F$) for the AF coating at 19 knots and 24 knots, respectively. Unfortunately, the study does not address the type of the applied coating.

At 19 knots, the maximum $\%\Delta C_F$ due to the FR, LPP and CDP coatings with low level hull roughness application was at least 3.4, 2.6 and 2 times respectively higher than the $\%\Delta C_F$ for the same type of coatings applied with normal finishes. Whereas the maximum $\%\Delta C_F$ for FR, LPP and CDP types with high level hull roughness were 5, 3.26 and 2.4 times higher in comparison to $\%\Delta C_F$ values for the same coatings with normal applications.

Another practical implication of the data presented lies in the traditional power prediction methods for new ships. The added frictional drag coefficients (ΔC_F) presented in Table 1 can be considered as an update for the 'roughness allowance', which is used for the trial power prediction of new ships. Historically, the American Towing Tank Conference (ATTC) recommended adding ΔC_F=0.0004 to the smooth surface friction coefficient (C_F) given by the Schoenherr line as the first guidance for the hull surfaces of new ships (Molland et al. 2011). A relationship for ΔC_F based on measured AHR of new ships proposed by Bowden and Davison (1974) (see Equation 2) and the Townsin (1985) formula (see Equation 3) which were adopted by the 15th (ITTC 1978) and 19th International Towing Tank Conference (ITTC 1990) respectively, have been used as a basis for the formulation of power penalties due to hull surface roughness.

$$\Delta C_F = \left[105\left(\frac{k_s}{L}\right)^{\frac{1}{3}} - 0.64\right] x10^{-3} \quad (2)$$

$$\Delta C_F = \left\{44\left[\left(\frac{k_s}{L}\right)^{\frac{1}{3}} - 10Re^{-\frac{1}{3}}\right] + 0.125\right\} x10^{-3} \quad (3)$$

In Equations 2 and 3, L is ship length and k_s is AHR of a ship. For practical purposes, ITTC (1978), in the absence of any measurement, recommended an approximate roughness value of k_s=150 × 10^{-6} m for a new ship's hull. Since 1985 there has been no new formula or relevant data proposed to estimate ΔC_F. Due to the introduction of new coating types and hull

surface applications, the need for such data has been emphasised on a number of occasions, especially at numerous ITTCs (eg Candries & Atlar 2002; Townsin 2002).

As demonstrated in Table 1, the predicted added drag, ΔC_F, for the KCS hull with the FR, LPP and CDP type with mimicked hull roughness finish changed from 0.000087 (FR-low1) to 0.000286 (CDP-high1) at 19 knots and from 0.000097 (FR-low1) to 0.000279 (CDP- high1) at 24 knots. It is interesting to note that these values of are still much lower than the traditional default value of roughness allowance for new ships, ΔC_F =0.0004.

Typical roughness allowances for the KCS were also derived using Equations 2 and 3 and compared with new ΔC_F values given in Table 1. In the equations, the k_s for each representative coating type and roughness density was taken to be equal to the R_t 50 values measured by using the TQC hull roughness gauge. Table 2 presents ΔC_F values calculated using the Bowden–Davison and Townsin formulas for the KCS case and percentage differences compared between the values derived using these two equations and current study results. In Table 2, percentage differences are given as absolute values of change in value, divided by the average of two numbers multiplied by 100.

By comparing ΔC_F values derived from the Bowden and Davison (1974) formula and current study results, it is clear that the formula estimates quite high roughness allowances for the KSC at two speeds, with FR, LPP and CDP types applied using mimicked hull roughness finishes. The percentage differences between ΔC_F values calculated using this equation and the values calculated in this study using the Granville's extrapolation procedure for modern-day typical FR types with mimicked hull roughness densities were significantly higher than for modern-day typical LPP and CDP types with mimicked hull roughness values.

The Townsin (1985) formula, incorporating Reynolds number effect, allowed estimation of roughness allowances for the KCS hull at slow steaming speed of 19 knots and design speed of 24 knots. Compared to ΔC_F values given in this paper for the KCS at 19 knots, the values obtained using the Townsin formula are significantly higher for FR type coatings with low and high roughness finishes. However, the Townsin formula closely follows the roughness allowances for LPP rather than CDP types with mimicked hull roughness densities at 19 knots. At 24 knots, the values derived using the Townsin formula fall within a reasonable range of ΔC_F values predicted in this study for CDP type coatings with low and high roughness finishes. The values estimated for the KCS with FR and LPP types with hull roughness densities and travelling at 24 knots design speed are significantly higher than the ΔC_F predictions given in this paper for the same coating types and coating finishes.

Apart from the above-described practical implications, the roughness characteristics and roughness functions for the coated surfaces investigated in this study can be built into the wall-functions of commercial CFD software as demonstrated by Demirel et al. (2017). This will provide more rational power estimations of ships by considering the three-dimensional effect on hull flows encountering more realistic surface conditions.

Conclusions

The experimental research presented set out to explore and demonstrate the effect on the performance of a ship from in-service hull conditions, namely the physical hull roughness in the presence of different coating types. The study concluded the following: (1) A new approach in mimicking hull roughness ranges provided an opportunity to acquire data on the typical roughness ranges observed on in-service ship hulls with modern popular AF coatings. The approach was developed based on a paint manufacturer's expertise and a database of hull roughness surveys. This work presents an initial pragmatic study in establishing the significance of low and high densities of sand grit roughness features on the performance of coatings. Extension of the work is needed for a better representation and understanding of physical in-service hull roughness such as a systematic study with an incremental range of roughness densities and magnitudes by replicating roughness from ships in-service. (2) Amongst the FR, LPP and CDP type coatings with mimicked hull roughness ranges in clean conditions, the study found a clear tendency, except for the FR types, for the drag increase (or skin friction coefficient, C_f) to be associated with the type of coating and the density of the roughness introduced in the coating scheme. At the highest tested *Re* number, the LPP and CDP coatings with high level hull roughness showed expected higher drag increase than the same coatings with low density of hull roughness. However, the drag performances displayed by the FR coatings with low and high density of roughness were not significantly different at the highest *Re* number.

(3) The roughness functions (ΔU^+) of the tested surfaces based on two test campaigns with normal and mimicked hull finishes, respectively, when plotted against the roughness Reynolds number (k^+), displayed a monotonic behaviour of the Colebrook-type Grigson roughness curve. The roughness length scales defined by the peak-to-trough height ($k = 0.14R_t$) and combination of root mean square roughness and spatial distribution of height parameters ($k = 0.4R_q\ (1+\lambda_a)^{0.05}$) presented a satisfactory correlation with $\Delta U^+$for coatings from both campaigns in the transitionally rough flow regimes. In this study, the latter roughness length scale was used for the first time, requiring further studies to explore the adequacy of the correlation for fully rough regimes. (4) Analysis of the measured roughness parameters, generated surface topographies and hydrodynamic drag data for FR, LPP and CDP type coatings with low and high density of physical roughness support the view that mimicked hull roughness has detrimental effects on the coating roughness and their frictional drag characteristics. Furthermore, for FR, LPP and CDP coatings, extrapolation of laboratory data to full-scale ship results emphasises the detrimental effects which greater roughness has on the ship resistance and powering penalties in comparison with estimations based on well-applied and relatively smooth coating conditions. This implies that current coating application guidance and practices may need re-assessment to reduce the hull roughness. (5) Formulae currently used for predicting ship roughness allowance (ΔC_F) do not represent modern hull coatings in terms of their types and surface finish. The present study has presented an update for such roughness allowance values which are applicable to modern commercial coatings combined with the mimicked physical hull roughness densities. The update indicates that the allowance values recommended by traditional methods are overestimated. The roughness and hydrodynamic data presented in this paper can be used in CFD codes to provide the basis for a more rational power estimation of ships by considering the three-dimensional hull flow effects in combination with more realistic treatment of the hull surface at various stages in life of the ship.

Acknowledgements

This research, which is based on the lead author's PhD study, was funded by International Paint Ltd (a division of Akzo-Nobel) and Newcastle University. Many thanks go to the Emerson Cavitation Tunnel team for their support during the experimental campaigns. Also, the authors would like to acknowledge the Marine coatings group at International Paint Ltd, especially Dr David Williams, Dr Barry Kidd and Dr Philip Stenson for their valuable input and Mr Harry Joyce for the application of the different coatings. The feedback and helpful comments of reviewers, as well as Mr Patrick Fitzsimmons's help during the write-up of this paper are also gratefully acknowledged.

Disclosure statement

No potential conflict of interest was reported by the authors.

Funding

This research was funded by International Paint Ltd (a division of Akzo-Nobel) and Newcastle University.

References

Atlar M, Seo K. 2011. Emerson Cavitation Tunnel Group of Newcastle University, UK. Bull Soc Naval architects Korea (BSNAK). 48:64–73.

B.S.R.A. 1980. Ship design manual/hydrodynamics. Chapter V(1).

Bayer RG. 1979. Wear tests for plastics: selection and use. American Society for Testing and Materials (ASTM). (ASTM Special Technical Publication 701).

Berendsen AM. 2013. Marine painting manual. New York: Springer Science and Business Media, B.V.

Bowden BS, Davison NJ. 1974. Resistance increments due to hull roughness associated with form factor extrapolation methods. NMI Ship TM 3800.

Candries M. 2001. Drag and boundary layer on antifouling paint [PhD thesis]. University of Newcastle-Upon Tyne, UK.

Candries M, Atlar M. 2002. Discussion on The Report Of The 23rd ITTC Resistance Commitee: Reconsideration of the correlation of roughness and drag characteristics of surfaces coated with antfoulings. Volume 1: The Resistance Commitee Final Report and Recommendations To The 23rd ITTC. Proceedings Of The 23rd ITTC-Volume 1; Venice, Italy.

Candries M, Atlar M. 2005. Experimental investigation of the turbulent boundary layer of surfaces coated with marine antifoulings. J Fluids Eng. 127:219–232. doi: 10.1115/1.1891148

Colebrook CF. 1939. Turbulent flows in pipes, with particular reference to transition region between smooth and rough pipe aalls. J Civil Eng. 11:133–157.

Coleman HW, Steele WG. 1999. Experimentation and uncertainty analysis for engineers. 3rd ed. Hoboken, NJ: John Wiley & Sons. Inc.

DANTEC. 2007. FlowExplorer installation and user's guide. Publication no:9040U2141. Dantec Dynamics A/S.

DeGraaff D. 1999. Reynolds-number scaling of the turbulent boundary layer on a flat plate and on swept and unswept bumps [PhD thesis]. Stanford University.

Demirel YK, Turan O, Incecik A. 2017. Predicting the effect of biofouling on ship resistance using CFD. Appl Ocean Res. 62:100–118. doi:10.1016/j.apor.2016.12.003

Dey SK. 1989. Parametric representation of hull painted surfaces and the correlation with fluid drag [PhD thesis]. University of Newcastle-Upon-Tyne.
Dürr S, Thomason JC. 2010. Biofouling. 1st ed. Hoboken (NJ): Blackwell Publishing Ltd.
Flack KA, Schultz MP. 2010. Review of hydraulic roughness scales in the fully rough regime. J Fluids Eng. 132: 041203–041210. doi:10.1115/1.4001492
Granville PS. 1958. The frictional resistance and turbulent boundary layer of rough surfaces. J Ship Res. 2:52–74.
Granville PS. 1987. Three indirect methods for the drag characterization of arbitarily rough surfaces on flat plates. J Ship Res. 31:70–77.
Grigson CWB. 1992. Drag losses of new ships caused by hull finish. J Ship Res. 36182–196.
Hama FR. 1954. Boundary-layer characteristics for smooth and rough surfaces. Soc Nav Arch Marine Engrs. 62: 333–351.
Haslbeck EG, Bohlander GS. 1992. Microbial biofilm effects on drag-lab and field. Proc SNAME Ship Production Symposium; New Orleans, Louisiana.
Hino T, (Ed). 2005. "Proceedings of CFD Workshop Tokyo". NMRI report 2005.
IMO. 2009. 9-April, Prevention of air pollution from ships: Second IMO GHG Study 2009. Marine Environment Protection. 59 session.
IMO. 2009. Prevention of air pollution from ships: Second IMO GHG Study 2009. Marine Environment Protection. 59 session.
ITTC. 1978. Proceedings of the 15th ITTC; Hague, Netherlands.
ITTC. 1990. Report on the Powering Performance Commitee. Proceedings of the 19th International Towing Tank Conference; Madrid.
Kim WJ, Van SH, Kim DH. 2001. Measurement of flows around modern commercial ship models. Experiments in Fluids. 31:567–578. doi:10.1007/s003480100332
Korkut E. 1999. An investigation into the scale effects on cavitation inception and noise in marine propellers [PhD thesis]. University of Newcastle Upon Tyne, UK.
Krogstad PA, Antonia RA, Browne LWB. 1992. Comparison between rough and smooth-wall turbulent boundary layers. J Fluid Mech. 245:599–617. doi:10.1017/S0022112092000594
Larsson L, Stern F, Visonneau M. 2014. Numerical ship hydrodynamics: an assessment of the Gothenburg 2010 Workshop. New York: Springer.
Medhurst JS. 1989. The systematic measurement and correlation of the frictional Rrsistance and topography of ship hull coatings, with particular reference to ablative antifoulings [PhD thesis]. University of Newcastle-Upon-Tyne.
Medhurst JS. 1990. Outline of a draft international standard for the measurement and characterization of roughness topography in fluid flow. Marine Roughness and Drag Workshop. Paper 11 (London).
Molland AF, Turnock SR, Hudson DA. 2011. Ship resistance and Ppopulsion: practical estimation of ship propulsive power. Cambridge, UK: Cambridge University Press.
Musker AJ. 1977. Turbulent shear flows near irregularly rough surfaces with particular reference to ships' hulls [PhD thesis]. University of Liverpool.
Nakao M. 1988. Senpaku no toso to toryo (Coating and paint for ships). In: The Ship Technology Society. p. 85–87.
Nikuradse J. 1933. Laws of flow in rough pipes. Washington: N.A.C.A Technical Memorandum 1292. Report No.
O'Leary C, Anderson CD. 2003. A new hull roughness penalty calculator the economic importance of hull condition: a collection of technical papers reprinted by International Marine Coatings.
Patel VC. 1965. Calibration of the preston tube and limitations on its use in pressure gradients. J Fluid Mech. 23: 185–205. doi:10.1017/S0022112065001301
Savio L, Ola Berge B, Koushan K, Axelsson M. 2015. Measurements of added resistance due to increased roughness on flat plates. The 4th International Conference on Advanced Model Measurement Technology for Maritime Industry (AMT'15); Istanbul, Turkey Hydro Testing Forum, 553–567.
Schultz MP. 2004. Frictional resistance of antifouling coating systems. Trans Asme, J Fluids Eng. 126:1039–1047. doi:10.1115/1.1845552
Schultz MP. 2007. Effects of coating roughness and biofouling on ship resistance and powering. Biofouling. 23: 331–341. doi:10.1080/08927010701461974
Schultz MP, Flack KA. 2003. Turbulent boundary layers over surfaces smoothed by sanding. J Fluids Eng. 125: 863–870. doi:10.1115/1.1598992
Schultz MP, Flack KA. 2007. The rough-wall turbulent boundary layer from the hydraulically smooth to the fully rough regime. J Fluid Mech. 580:381–405. doi: 10.1017/S0022112007005502
Stenson P, Kidd B, Chen H, Finnie A, Ramsden R. 2014. Predicting the impact of hull roughness on the frictional resistance of ships. International Conference on Computational and Experimental Marine Hydrodynamics; Chennai, India (MARTHY 2014 Conference Proceedings), Vol. 2; Chennai, India. p. 44–51.
Stenson P, Kidd B, Finnie A. 2013. Measurement and impact of surface topology and hydrodynamic drag of fouling control coatings. Proceedings of the 3rd International Conference on Advanced Model Measurement Technology for the Maritime Industry (AMT'13); Hydro Testing Forum; Gdansk, Poland: p. 384–396.
Swinscow TDV, Campbell MJ. 2002. Statistics at square sne. 10th ed. London: BMJ Books.
Tezdogan T, Demirel YK, Kellett P, Khorasanchi M, Incecik A, Turan O. 2015. Full-scale unsteady RANS CFD simulations of ship behaviour and performance in head seas due to slow steaming. Ocean Engineering. 97: 186–206. doi:10.1016/j.oceaneng.2015.01.011
Thomas RT. 1999. Rough surface. 2nd. ed. London, UK: Imperial College Press.
Townsin RL. 1985. The ITTC Line - it's genesis and correlation allowance. The Naval Architect, RINA.E359-E362.
Townsin RL. 2002. Discussion on the Report Of The 23rd ITTC Resistance Commitee: Rooughness and the ITTC correlation allowance - a new problem. Proceedings Of The 23rd ITTC - Volume 1 The Resistance Committee Final Report and Recommendations to the 23rd ITTC; Venice, Italy.
Townsin RL. 2003. The dhip hull fouling penalty. Biofouling. 19:9–15. doi:10.1080/0892701031000088535
TQC. 2018. TQC Hull Roughness gauge. [accessed]. https://www.tqc.eu.

Unal B. 2012. Effect of surface roughness on the turbulent boundary layer [PhD thesis]. Istanbul Technical University.
Unal O. 2015. Correlation of frictional drag and roughness length scale for transitionally and fully rough turbulent boundary layers. Ocean Engineering. 107:283–298. doi: 10.1016/j.oceaneng.2015.07.048
Volino RJ, Schultz MP, Flack KA. 2007. Turbulence structure in rough-and smooth wall boundary layers. J Fluid Mech. 592:263–293.
Yeginbayeva IA. 2017. An investigation into hydrodynamic performance of marine coatings 'in-service' conditions [PhD thesis]. Newcastle, UK: Newcastle University.